



# Constraining the hydration of the subducting Nazca plate beneath Northern Chile using subduction zone guided waves



Tom Garth\*, Andreas Rietbrock

Department of Earth, Ocean and Ecological Sciences, University of Liverpool, United Kingdom

## ARTICLE INFO

### Article history:

Received 28 March 2017

Received in revised form 23 June 2017

Accepted 25 June 2017

Available online xxxx

Editor: P. Shearer

### Keywords:

subduction zones

South America

Wadati–Benioff zones

guided waves

## ABSTRACT

Guided wave dispersion is observed from earthquakes at 180–280 km depth recorded at stations in the fore-arc of Northern Chile, where the 44 Ma Nazca plate subducts beneath South America. Characteristic P-wave dispersion is observed at several stations in the Chilean fore-arc with high frequency energy (>5 Hz) arriving up to 3 s after low frequency (<2 Hz) arrivals. This dispersion has been attributed to low velocity structure within the subducting Nazca plate which acts as a waveguide, retaining and delaying high frequency energy. Full waveform modelling shows that the single LVL proposed by previous studies does not produce the first motion dispersion observed at multiple stations, or the extended P-wave coda observed in arrivals from intermediate depth events within the Nazca plate. These signals can however be accurately accounted for if dipping low velocity fault zones are included within the subducting lithospheric mantle. A grid search over possible LVL and faults zone parameters (width, velocity contrast and separation distance) was carried out to constrain the best fitting model parameters. Our results imply that fault zone structures of 0.5–1.0 km thickness, and 5–10 km spacing, consistent with observations at the outer rise are present within the subducted slab at intermediate depths. We propose that these low velocity fault zone structures represent the hydrated structure within the lithospheric mantle. They may be formed initially by normal faults at the outer rise, which act as a pathway for fluids to penetrate the deeper slab due to the bending and unbending stresses within the subducting plate. Our observations suggest that the lithospheric mantle is 5–15% serpentinised, and therefore may transport approximately 13–42 Tg/Myr of water per meter of arc. The guided wave observations also suggest that a thin LVL (~1 km thick) interpreted as un-eclogitised subducted oceanic crust persists to depths of at least 220 km. Comparison of the inferred seismic velocities with those predicted for various MORB assemblages suggest that this thin LVL may be accounted for by low velocity lawsonite-bearing assemblages, suggesting that some mineral-bound water within the oceanic crust may be transported well beyond the volcanic arc. While older subducting slabs may carry more water per metre of arc, approximately one third of the oceanic material subducted globally is of a similar age to the Nazca plate. This suggests that subducting oceanic lithosphere of this age has a significant role to play in the global water cycle.

© 2017 The Authors. Published by Elsevier B.V. This is an open access article under the CC BY license (<http://creativecommons.org/licenses/by/4.0/>).

## 1. Introduction

Subducting oceanic crust is widely thought to deliver large amounts of water to the mantle, some of which is thought to be released from the slab (causing intermediate depth earthquakes) and rise through the mantle wedge to cause arc volcanism. This release of water is thought to occur as hydrous mineral assemblages lose their bound water through metamorphic reactions due to increased temperature and pressure. Some water however is car-

ried to greater depths by meta-stable oceanic crust and hydrated minerals in the subducting lithospheric mantle. Observations of the hydrated structure of the oceanic plate at intermediate depths, where dehydration processes take place, are however limited. This is largely due to the lack of resolution of conventional seismic imaging methods (e.g. seismic tomography) at these depths.

Subduction zone guided wave observations have the potential to probe the fine scale structure of the down-going plate, and hence constrain the onset of these dehydration reactions, due to the large amount of time these trapped waves spend interacting with the subducting slab. Observations of guided wave dispersion from a number of subduction zones around the Pacific suggest that upper plane intermediate depth earthquakes may be asso-

\* Corresponding author.

E-mail address: [tomgarth@liverpool.ac.uk](mailto:tomgarth@liverpool.ac.uk) (T. Garth).

ciated with low velocity hydrated minerals that have not transformed to eclogite in the subducted oceanic plate (Abers, 2000; Martin et al., 2003). Detailed analysis of guided wave observations from upper plane Wadati–Benioff zone (WBZ) events in Northern Japan suggest that low velocity hydrated mineral assemblages may persist to much greater depths than is predicted by thermal and petrological modelling of these dehydration reactions (Garth and Rietbrock, 2014a). Observations from lower plane WBZ seismicity in Northern Japan also suggest that these events may be directly associated with low velocity channels, caused by serpentinised outer rise normal faults that penetrate the subducting slab mantle (Garth and Rietbrock, 2014a, 2014b).

Outer rise faulting has been proposed as an effective method of hydrating the lithospheric mantle and accounting for the occurrence of lower plane WBZ seismicity through dehydration processes (e.g. Peacock, 2001). Seismic reflection profiles have shown the presence of outer rise faults penetrating the lithospheric mantle in Nicaragua (Ranero et al., 2003) and Central Chile (Grevemeyer et al., 2005) and an associated drop in heat flow due to the onset of serpentinisation is observed at the outer rise in both of these subduction zones (Grevemeyer et al., 2005). More recently the hydrated zone where these dipping outer rise normal faults penetrate the oceanic crust has been constrained in Nicaragua using electromagnetic methods (Naif et al., 2015), showing that the geometry of the hydrated structure is controlled by the outer rise faults. Geodynamic modelling of the formation of outer rise normal faults suggests that the extent to which these faults penetrate into the subducting plate may increase with depth within the subduction zone, as fluids are forced down as the subducting slab unbends (Faccenda et al., 2009, 2012). These models demonstrate the mechanism by which the lithospheric mantle may become hydrated, allowing lower plane WBZ seismicity to occur due to the associated dehydration reactions.

In Northern Chile outer rise faulting is apparent from the bathymetry of the oceanic plate close to the trench (Fig. 1). Constraints from refraction tomography and gravity inversion in the area suggest that at the trench an approximately 20 km thick layer of hydrated lithospheric mantle is present beneath the subducting oceanic crust (Ranero and Sallares, 2004). It is proposed that these outer rise normal faults (and other structures within the subducting plate) are reactivated in the WBZ (Rietbrock and Waldhauser, 2004; Ranero et al., 2005), suggesting that these fault zone structures persist to intermediate depths within the subduction zone.

Analysis of guided waves from intermediate depth earthquakes in Northern Japan has shown that low velocity hydrated fault zone structures persist to depths of up to ~150 km and can therefore account for lower plane WBZ seismicity. Additionally, analysis of the P-wave coda from these events provides a constraint on the hydration of the subducted lithospheric mantle, showing that this part of the subducting slab is highly hydrated and carries approximately 90% of the water transported to the mantle (Garth and Rietbrock, 2014b).

This study concerns the South American subduction zone in Northern Chile, where the 44 Myr Nazca plate is subducted beneath the South American plate at approximately 78 mm/yr (van Keken et al., 2011). This much younger and therefore warmer subducting oceanic crust contrasts with the 130 Myr cooler oceanic crust subducting in Northern Japan (Garth and Rietbrock, 2014a, 2014b). Our results therefore provide a test of whether the low velocity features observed in Northern Japan are unique to older subducting oceanic plates or are more ubiquitous feature of subduction zones with a variety of ages and thermal properties. The results also provide crucial information about how much water is transported by the lithospheric mantle in ‘younger’ subduction zones and therefore provides vital evidence for estimating the overall water budget in the Earth’s mantle.

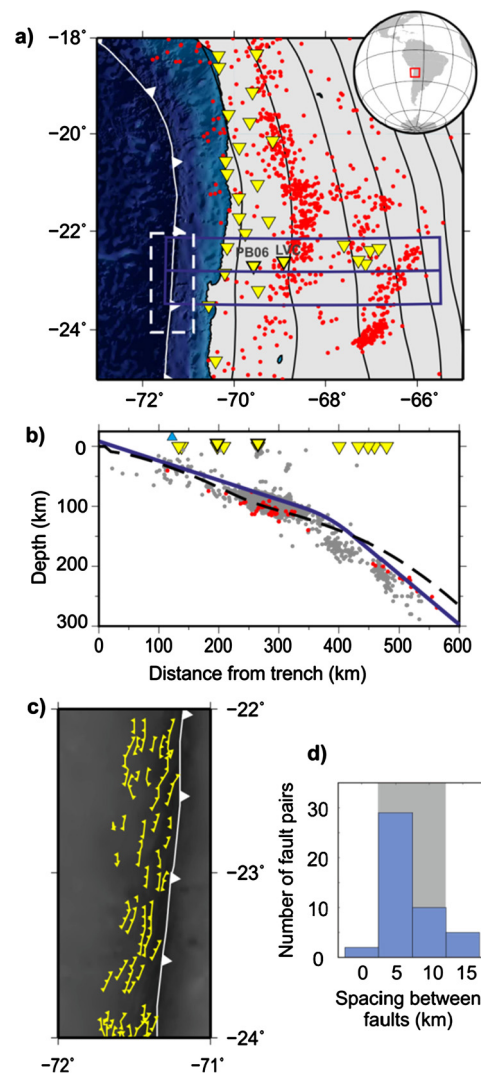


**Fig. 1.** Summary map and profile. **a)** The study area of Northern Chile. Well located background seismicity from the ISC earthquake bulletin from 2010–2014 (International Seismological Centre, 2014) is shown in red, and slab contours are shown from slab1.0 (Hayes et al., 2012). The IPOC broadband seismic network (GFZ German Research Centre for Geosciences, 2006), temporary stations used in Bolivia (West and Christensen, 2010), and IU station LVC are shown by the inverted yellow triangles. The stations used in the grid searches are highlighted and labelled. The blue box shows the profile location given in the bottom panel. **b)** Local seismicity located with temporary networks is shown in grey, and well located events from the ISC bulletin are shown in red. The slab geometry of slab1.0 (Hayes et al., 2012) is indicated by the dashed black line and the chosen model geometry is given by the blue line. The blue triangle shows the location of the coast. **c)** Bathymetry is shown in grey, with the outer-rise fault structures identified by Ranero et al. (2005) highlighted in yellow. The area plotted is shown by the dashed white box in a). **d)** A histogram showing the number of faults with specific fault spacing. (For interpretation of the references to colour in this figure legend, the reader is referred to the web version of this article.)

Subduction zone guided waves have previously been observed in the study area from temporary seismic deployments (Martin et al., 2003, 2005; Martin and Rietbrock, 2006), and studies suggest that a relatively thin (<4.5 km thick) low velocity layer (LVL) persists to a depth of at least 160 km (Martin et al., 2003). Guided wave arrivals are seen as energy decouples from the slab due to the bend of the slab (Martin et al., 2003; Martin and Rietbrock, 2006), and at shallower depths due to contact with the low velocity over riding plate (Martin et al., 2005). In this paper we present new guided wave observations from the South American subduction zone, recorded on permanent broadband stations in Northern Chile. We explore the new resolution

that can be gained by constraining the guided wave dispersion with full waveform models, adapting the techniques developed in previous subduction zone guided wave studies in Northern Japan (Garth and Rietbrock, 2014a, 2014b).

We show that dispersed arrivals recorded in Northern Chile cannot be explained solely by a single LVL as such a model cannot account for the extended P-wave coda observed at stations close to the trench where the decoupled guided wave is observed. However, the addition of dipping low velocity normal fault structures not only accounts for the extended P-wave coda, but also allows the clear dispersion of P-wave arrivals observed to be accurately simulated.

## 2. Guided wave observations

Guided wave arrivals are observed at stations in the subduction zone fore-arc in the Antofagasta region of Northern Chile. In this area prevalent WBZ seismicity is present to depths of up to ~300 km (Fig. 1) and guided wave arrivals are observed on permanent broadband seismometers from the Global Seismic Network (GSN) and the Integrated Plate Observatory Chile (IPOC) (GFZ German Research Centre for Geosciences, 2006). Additional stations from the temporary seismic array in Southern Bolivia (West and Christensen, 2010) are used to give an overview of the development of the guided waves arrivals observed across the arc.

The characteristic dispersion observed at stations PB06 and LVC for events at 180–280 km depth is shown in Fig. 2. The high frequency arrivals are delayed by several seconds, with the delay increasing with the depth of the source. As a typical example of the available data Fig. 2 shows the first ten intermediate-depth earthquakes to occur during 2010, with additional selected events to fill gaps in the depth profile. Due to the large number of intermediate depth events in this part of Chile, it is not possible to show all events for a larger time span. Events showing the clearest dispersion are then used for further analysis.

### 2.1. Local seismicity

In many subduction zones it is noted that the depth of WBZ events is underestimated by global catalogues when compared to local catalogues (Syracuse and Abers, 2006). In Northern Chile well constrained earthquake locations from dense temporary seismic deployments in the region (e.g. Martin et al., 2003) show far less scatter and systematically plot deeper than the global PDE catalogue. In this study the slab geometry is therefore constrained using the accurate locations from the dense temporary networks. In addition, we select events from the ISC bulletin (International Seismological Centre, 2014) that are located using four or more depth phase observations to increase depth accuracy. The depth range of these events is in good agreement with the depth range of events from the dense temporary networks as shown in Fig. 1. Locations from the PDE catalogue are used to identify potential events that may show guided wave dispersion, so events are not ruled out if there are no clear depth phases. For the purpose of modelling, it is assumed that these earthquakes occur close to the well constrained slab geometry, effectively correcting the depth of these events.

### 2.2. Guided wave dispersion observations

Guided waves are identified using a Gaussian taper spectrogram to determine the relative arrival times of different frequency components of the dispersed P-wave arrival (Abers, 2000, 2005; Garth and Rietbrock, 2014a, 2014b). The spectrogram is plotted at 0.25 Hz intervals from 0.25–12 Hz, as shown in Fig. 3. Dispersed arrivals are seen from events at intermediate depths within the

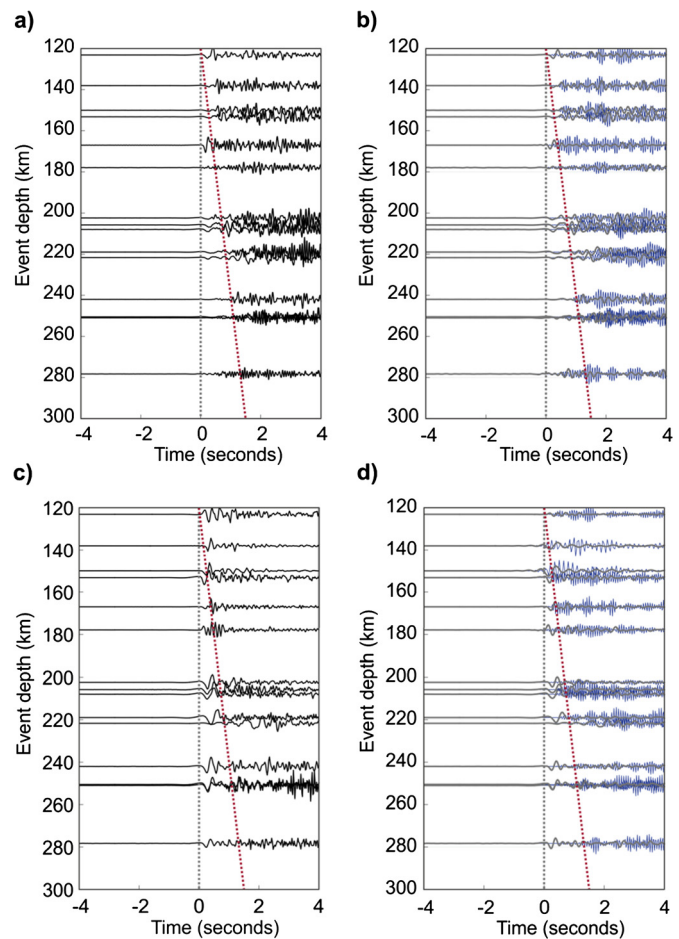


**Fig. 2.** Waveform depth profile. **a)** The z-component data recorded at station PB06 for events at different depths on the profile shown in Fig. 1. **b)** The low-pass filtered waveforms (<5 Hz) in grey and high-pass filtered waveform (>12 Hz) in blue recorded at station PB06. On both panels the waveforms are aligned to the first arrival, which is shown by the grey dashed line. The delayed high frequency arrival is shown by the red dashed line. **c)** Shows the unfiltered waveform for the same events recorded at the station LVC, and **d)** shows the events recorded at LVC filtered as described in b). (For interpretation of the references to colour in this figure legend, the reader is referred to the web version of this article.)

WBZ, with higher frequencies (>5 Hz) delayed by 1–3 s. It is noted that the lowest frequency that is delayed by a second or more is significantly higher in this setting than for similar observations in Northern Japan (Garth and Rietbrock, 2014a, 2014b) and other subduction zones (Abers, 2000, 2005).

Guided wave dispersion is observed at stations in the fore-arc as the high frequency energy decouples due to the bend of the subducting slab (Martin et al., 2003; Martin and Rietbrock, 2006). Therefore we would only expect to see clear decoupled guided waves and the associated dispersion in a specific window within the fore-arc. The delay of high frequency arrivals increases with depth within the subduction zone for arrivals recorded at both stations PB06 and LVC, as the high frequency guided wave from deeper events interact with the low velocity structure in the subducting slab for longer. At other stations in the IPOC network that are closer to the coast, dispersion is seen less clearly as they are further from the ‘decoupling window’. Arrivals at these stations may also be affected by guided wave energy that has decoupled due to contact with the overriding plate. Outside of the decoupling window (>350 km from the coast) a much sharper P-wave arrival with no strong coda is seen in both the models and the recorded data as shown in Fig. 4.



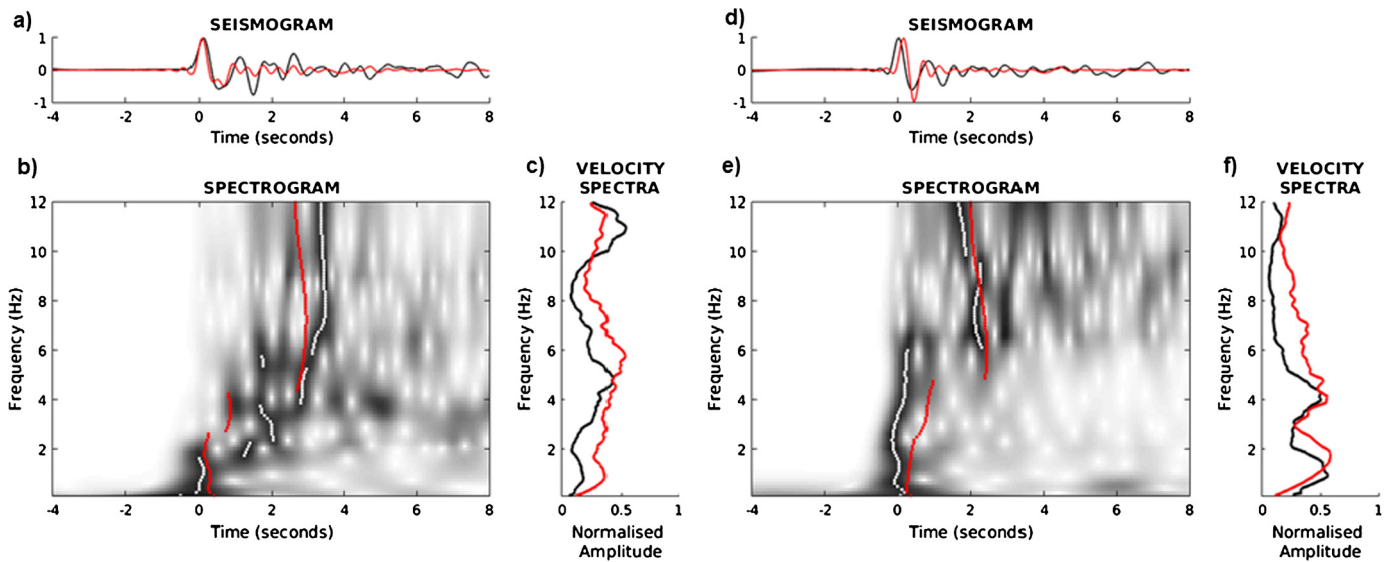


**Fig. 3.** Comparison between observed dispersive waveforms (shown in black and white) and synthetic observed waveforms (shown in red) for the station PB06 (left) and LVC (right). **a)** The low pass filtered ( $<2$  Hz) observed (black) and modelled (red) waveforms for station PB06. **b)** The observed spectrogram is shown in black and white, while the arrival time of the maximum energy at a given frequency of the modelled spectrogram is shown in red. **c)** The observed (black) and modelled (red) velocity spectrum are compared. **d), e)** and **f)** show the low pass filtered waveforms, spectrogram, and velocity spectrum compared for the station LVC. (For interpretation of the references to colour in this figure legend, the reader is referred to the web version of this article.)

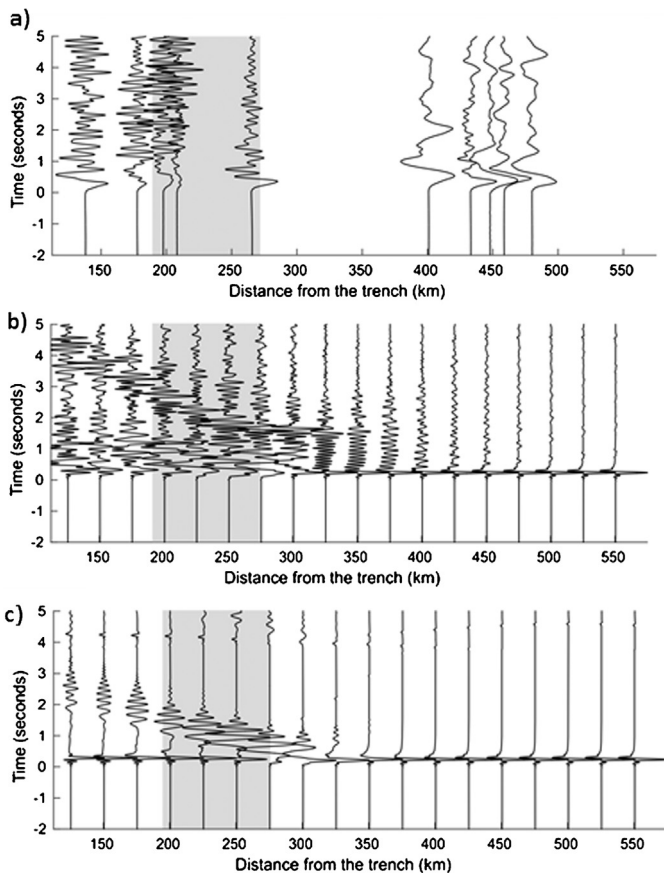


**Fig. 4.** Development of the wave field with distance from the trench. **a)** The observed wave-field from an event at 220 km depth recorded on stations across the volcanic arc. **b)** The wave-field from a model that includes dipping fault zones. **c)** The wave field from a velocity model with a single LVL. It is noted that the strong coda noted from intermediate depth events recorded in the Chilean for arc is only seen when the fault zone structures are included. Synthetic waveforms are shown from the offset of the coast to 550 km distance from the trench. The approximate offset of the stations in the fore-arc is shown in grey.

The nature of the dispersed arrivals observed at stations PB06 and LVC also differs as the two sites are located at different offsets from the slab bend and therefore sample different proportions of the guided and direct wave-field. The dispersed arrivals for a single event at 218 km depth, recorded at both PB06 and LVC are shown in Fig. 3. The observed waveform is shown in black and white, while the synthetic waveform shown in red as described in more detail in section 4.

Although both waveforms are from the same event, the arrivals look markedly different due to their position within the decoupling window. At station LVC we do not see the full characteristic dispersion that is often associated with subduction zone guided wave arrivals. In the spectrogram we see a relatively undispersed arrival until  $>6$  Hz, after which higher frequency energy that is delayed by  $\sim 2$  s arrives. In addition the velocity spectra show that the signal appears to be dominated by low frequency energy. This suggests that the high frequency energy that is retained within the waveguide has not fully decoupled and so is not dominant in the wave-field observed at this point in the fore-arc.

A more clearly dispersive signal is seen for the same event at the station PB06. The spectrogram shows that frequencies below 2 Hz are un-delayed, frequencies above 6 Hz are fully delayed, while intermediate frequencies (between 2–6 Hz) become progressively more delayed with increasing frequency. The velocity spectrum of the signal at PB06 shows that there is far more high frequency energy at this station, as it is further into the decoupling window where the decoupled guided wave energy is seen. This progressive onset of observed guided wave dispersion with distance up-dip of the decoupling point is captured in the synthetic models shown in Fig. 3.

The spectrogram gives a first order indication of the low velocity structure, with low frequencies ( $<2$  Hz) arriving first as they are relatively unaffected by the low velocity structure. Intermediate frequencies (2–6 Hz) become progressively more delayed with increasing frequency, and high frequencies ( $>6$  Hz) are fully delayed, as the wavelengths are small compared to low velocity structures such as the LVL and faults within the subducting slab.

### 3. Modelling and constraining subduction zone guided waves

The dispersed guided wave arrivals are simulated using the 2D finite difference (FD) full waveform modelling software *sofi2D* (Bohlen, 2002). This leads on from previous studies that have used full waveform modelling to simulate the effect of the subduction zone waveguide on the frequency content of the dispersed signal (Martin et al., 2003; Martin and Rietbrock, 2006), the extended P-wave coda of the signal (Garth and Rietbrock, 2014a; Furumura and Kennett, 2005), and the delay of the high frequency arrivals (Garth and Rietbrock, 2014a, 2014b).

Here we employ the methodology developed by Garth and Rietbrock (2014a, 2014b), which combines these approaches and constrains the guided wave arrival in both the frequency domain, using the velocity spectra, and the frequency-time domain using a spectrogram. We also consider the extended P-wave coda that is seen in the Chilean fore-arc, to add additional constraints on the low velocity structure at depth.

#### 3.1. Waveform model setup

The synthetic waveforms are calculated up to a frequency of 12 Hz by a 2D FD waveform propagation model with a 25 m grid spacing (Bohlen, 2002). Simulations are carried out with an explosive spike seismic source to simulate the entire P-wave spectrum. Intermediate depth seismicity in the subducting Nazca plate is dominated by down-dip extensional earthquakes (e.g. Rietbrock and Waldhauser, 2004), and it has been shown that an explosive source is a good approximation of the up dip P-wave radiation pattern (Martin and Rietbrock, 2006). The seismic source is positioned in the centre of the LVL, as synthetic tests show that for the velocity model proposed, guided wave dispersion is seen most clearly when the source is located within the lower two thirds of the LVL. Source positions in the upper third of the LVL show minimal change in the overall waveform and velocity spectra, however the position of the source does affect the relative amplitude of the guided wave and other phases (Martin and Rietbrock, 2006) hence affecting the clarity of the dispersion. Simulations are carried out in an elastic medium as the P-wave attenuation in the Chilean fore-arc has been shown to be very low (e.g. Schurr et al., 2003), and previous guided wave studies have shown that the effect of elevated attenuation in the subduction zone system are minimal (Garth and Rietbrock, 2014a).

#### 3.2. Inferring velocity model

The velocities of the subducting slab, surrounding mantle, and overriding plate are based on local tomographic studies of the area (Schurr et al., 2003; Graeber and Asch, 1999). A thin LVL overlies the fast slab, as proposed by previous guided wave studies in the area (Martin et al., 2003, 2005; Martin and Rietbrock, 2006). The velocity model also includes dipping low velocity fault zone structures, similar to those inferred in Northern Japan (Garth and Rietbrock, 2014b). The thickness and velocity contrast of the LVL is varied, along with other parameters such as fault spacing and thickness. The resulting waveforms are then compared to the observed waveforms to constrain the characteristics of the low velocity structure within the subducted slab.

The velocity model is shown in Fig. 5, along with snapshots of the developing wave-field. Fig. 5b shows how seismic energy interacts with the proposed low velocity structures within the slab. High frequency energy is retained within the low velocity waveguide and decouples from the waveguide due to the bend of the slab e.g. Martin et al. (2003). This produces the dispersed arrivals in the guided wave decoupling window that is approximately

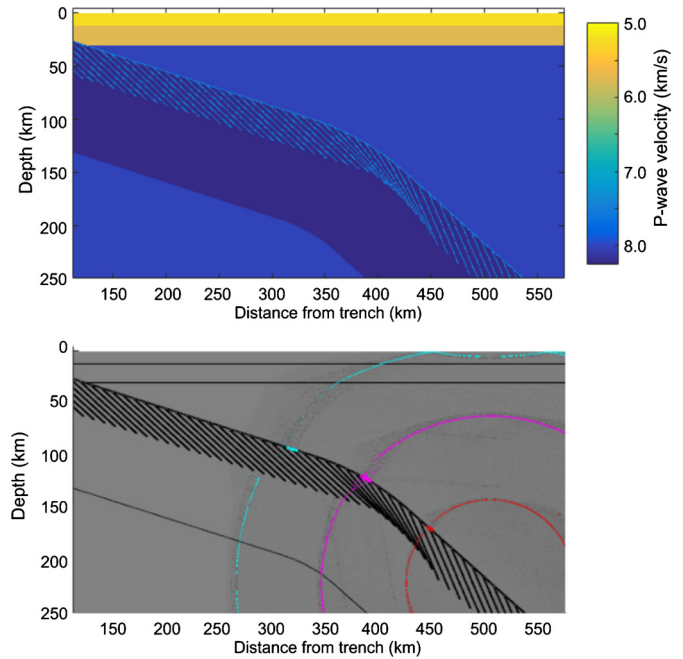


**Fig. 5.** a) The p-wave velocity model proposed to represent the hydrated oceanic crust subducting beneath Northern Chile. b) Snapshots of the dispersive wave-field highlighted in red, pink and blue at 10, 20 and 30 s respectively. The outline of the velocity model above is shown by the black contours. (For interpretation of the references to colour in this figure legend, the reader is referred to the web version of this article.)

100–300 km from the trench. Sharper undispersed arrivals are observed further from the trench, as these seismic waves have not interacted with the low velocity structure of the slab (Fig. 4).

#### 3.3. Waveform comparison

The methods developed by Garth and Rietbrock (2014a) are used to constrain the dispersed guided wave arrivals recorded in the Chilean fore-arc. The relative arrival time of the peak energy in each frequency band of the spectrogram is compared to give the spectrogram misfit. The normalised amplitudes of the velocity spectra of the observed and modelled waveform are compared in order to give the velocity spectra misfit and constrain the relative amplitude of the different frequency bands. Using these two respective methods to determine the relative arrival time and amplitude at a given frequency respectively, allows the full dispersive waveform to be directly constrained. The synthetic and observed dispersed waveforms, low pass filtered at 2.5 Hz, are then compared providing additional constraint on the phase of the low frequency part of the waveform.

These three measures of misfit are then combined into a normalised overall misfit value following Garth and Rietbrock (2014a). The combined misfit is calculated with a 40% weighting on each of the spectrogram and velocity spectra misfits ( $M_{spec}$  and  $M_{velspec}$  respectively) and a 20% weighting on the misfit of the low pass filtered waveform ( $M_{wave}$ ), using the formulation shown below.

$$\text{Combined Misfit} = \frac{40(M_{spec}) + 40(M_{velspec}) + 20(M_{wave})}{100}$$

Equal weighting is given to both the spectrogram and velocity spectra as they are sensitive to different features of the velocity structure. Comparing both measures of the dispersed waveform gives a tighter constraint on the velocity structure and removes potential trade-offs between the velocity and width of the waveguide (Garth and Rietbrock, 2014a). The misfit of the waveform is given

a lower weighting as it has been low pass filtered at 2.5 Hz and therefore the high frequency part of the wave-field is neglected.

#### 4. Constraining the low velocity structure of the slab

The combined misfit is used to inform a grid search for the properties of the low velocity structures in the subducted slab. A range of potential parameters are tested to constrain the average velocity of the low velocity structure, the thickness of the LVL, as well as the thickness and spacing of the low velocity faults structure within the lithospheric mantle. The misfit between the observed waveforms and synthetic waveforms produced for each velocity model can then be used to constrain the low velocity structure present in the down-going slab.

Initially the guided wave observations presented here were tested against the optimum single LVL model proposed to explain guided wave observations in this region (Martin et al., 2003; Martin and Rietbrock, 2006). A cross-section comparing the waveforms produced by this velocity model with recorded waveforms from across the fore-arc is shown in Fig. 4. The decoupled guided arrivals can be seen at distances of less than  $\sim 300$  km from the trench. The waveforms are however dominated by a sharp first arrival that is not seen in the guided wave dispersion observations.

While some evidence of dispersion is present in the spectrogram for the single LVL model, this model does not account for the clear delay of the higher frequency at stations PB06 or LVC, in the fore-arc. The waveform is dominated by the undispersed first arrival of a refracted phase travelling below the oceanic Moho of the subducted slab. The single LVL model also does not recreate the extended P-wave coda associated with arrivals from intermediate depth earthquakes recorded in the Chilean fore-arc (Fig. 4).

We therefore test velocity models including dipping low velocity normal fault structures, as inferred within the subducted lithospheric mantle of Northern Japan (Garth and Rietbrock, 2014b) and imaged at the outer rise in several subduction zones e.g. (Ranero et al., 2003; Grevemeyer et al., 2005; Naif et al., 2015). These low velocity structures within the upper lithospheric mantle of the subducted slab dissipate the refracted phase, reducing its relative amplitude. This allows the characteristic dispersion associated with the guided wave arrival to be accurately simulated at fore-arc stations in models that include dipping low velocity fault zones. The addition of dipping low velocity fault zones in the velocity model also recreates the strong P-wave coda noted at stations across the Chilean fore-arc (Fig. 4).

Previous studies have shown that a random scattering media in the subducted plate can account for the extended P-wave coda from intermediate depth earthquakes (Garth and Rietbrock, 2014b; Furumura and Kennett, 2005). However we find that only a sharp and strong velocity contrast within the lithospheric mantle is able to explain the observed amplitude ratio between refracted and guided wave arrivals shown in Fig. 2. We propose that this strong velocity contrast is due to low velocity structure associated with fault zones that are present at intermediate depths within the subducted slab.

##### 4.1. Grid search for low velocity structure

In order to constrain the low velocity structure of the subducting slab, we must consider variations in the structure of both the upper LVL and the low velocity fault structures proposed here. In order to do this we construct a large scale grid search to constrain the proposed intermediate depth low velocity structures in the subducted Nazca plate. We test a range of average velocities for the low velocity structure between 7.2 and 7.8 km/s, and a range of LVL widths between 0.5 and 4.0 km. In addition, a range of fault zone spacings of between 2.5 and 10.0 km and fault zone widths

between 0.25 and 2.0 km are tested. The dip of the fault zones is fixed at  $25^\circ$  relative to the surface of the down going plate and for simplicity an average velocity is set for the whole of the proposed low velocity structure. In the models presented, the length of the faults is assumed to be 75 km, meaning they penetrate to a depth of  $\sim 35$  km below the slab surface. A range of fault lengths have been tested to investigate the effect of the depth extent of the hydrated fault zones on the synthetic waveforms. We find that varying the depth extent of the faults and therefore the thickness of the hydrated zone has no significant effect on the observed dispersion. The position of the source within the LVL is shown to have a minimal effect on the overall dispersion seen, but most dispersion is seen if the source is in the lower portion of the LVL. The source is therefore fixed to the centre of the LVL, as described in section 3.1. The resulting grid space is shown in Fig. 6, where the average of the combined misfit at stations PB06 and LVC is shown for the range of models. The grid of models shows that the best fitting dispersion is seen for events that have a fault spacing of 5.0–10.0 km, and a fault width of 0.5–1.0 km. For each of these models the average velocity of the proposed low velocity structures is constrained to be 7.4–7.6 km/s, and the thickness of the overriding LVL is tightly constrained to 1 km.

In order to better understand the range of parameters that fit the dispersion, two slices are taken through the parameter grid. Fig. 7 shows a slice through the grid demonstrating the variation in misfit due to varying the LVL width and the average velocity of the low velocity structure, assuming a fault zone width of 1 km and fault zone spacing of 10 km. Fig. 8 shows a slice through the parameter grid showing the resolution of the low velocity fault zone structure, assuming a fixed average velocity of 7.5 km/s, and a LVL thickness of 1 km. In both Fig. 7 and 8 the model misfit for each of the stations considered is shown.

The subsection shown in Fig. 7 demonstrates that the width of the LVL is tightly constrained to 1 km, and that the bulk velocity of the fault zone structure is constrained to 7.4–7.6 km/s. For both stations the spectrogram fit favours a slightly slower seismic velocity than the velocity spectra. Overall the structure of the LVL is more tightly constrained at the station PB06 than at station LVC, though the best fitting models are in good agreement. This range of possible velocities is confirmed by the full misfit grid shown in Fig. 6. The thin LVL inferred here is consistent with the single LVL structure proposed in previous studies in the area (e.g. Martin et al., 2003).

The subsection of the model space shown in Fig. 8 shows the range of different faulting models that can potentially explain the observed P-wave dispersion. For both stations considered there is notable agreement in the best fitting models between the spectrograms and velocity spectra, while the low-pass filtered waveform fit seems less sensitive to this structure. The dispersion observed at station LVC is explained by a wider range of fault zone structures than the station PB06. However, the dispersion constrained at both stations is consistent with low velocity fault zone structures of 0.5–1.0 km width, with a spacing of 5–10 km. This spacing is consistent with the spacing of fault scarps apparent in the bathymetry at the outer rise which have a range of spacing from 2.5–10 km (Grevemeyer et al., 2005; Ranero et al., 2005), as shown in Fig. 1.

##### 4.2. Waveform fits

The synthetic waveforms produced by the best fitting model are directly compared to the dispersed waveforms observed at station PB06 and LVC in Fig. 3. The model shown has a fault spacing of 10 km, a fault width of 1.0 km, a LVL width of 1.0 km, and the low velocity structure has a velocity of 7.5 km/s. Fig. 9 shows a comparison of waveforms produced using the best fitting velocity model



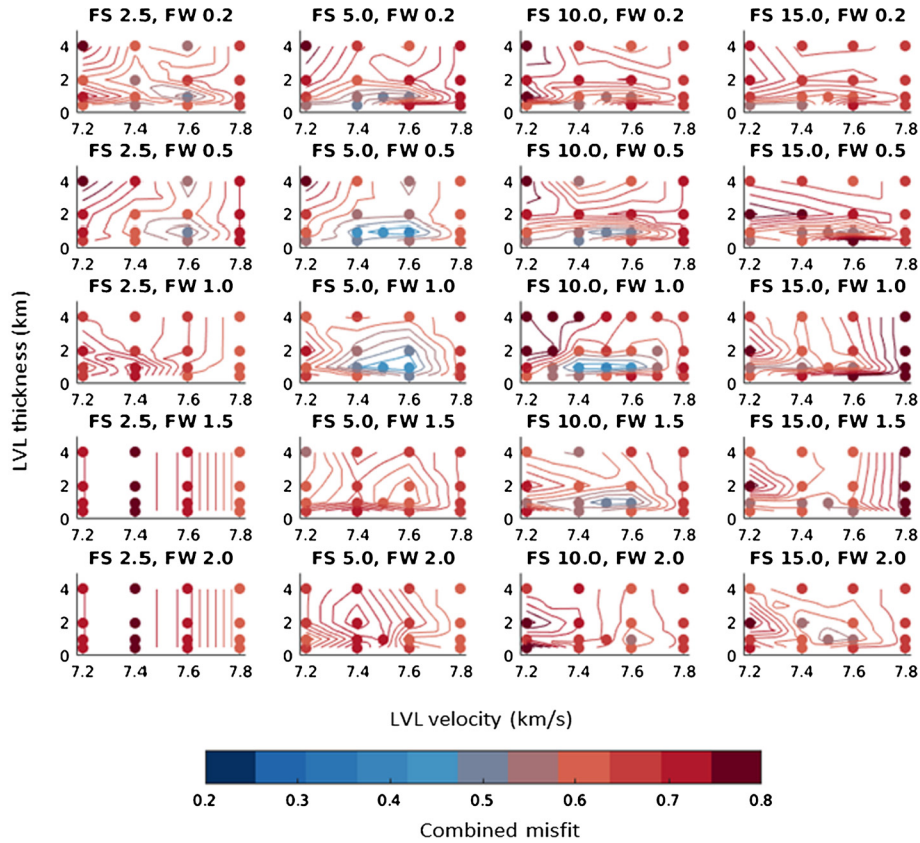


**Fig. 6.** Combined misfit of synthetic waveforms to the observed dispersion observed at the stations PB06 and LVC. Each panel shows models with a different fault spacing (FS) and fault width (FW) quoted in kilometres. For each panel a variety of average velocities (x-axis) and LVL thicknesses (y-axis) are tested. The grid search shows that a similar range of low velocity layer characteristics produce the best fitting model, regardless of the fault zone parameters, and there is no clear trade-off between the fault zone and LVL structures.

with dispersed arrivals recorded at station PB06, from earthquakes at depths between 140 and 220 km.

The spectrogram of these events shows that the delay of the high frequencies increases with earthquake depth, as shown for a wider range of events in Fig. 2. The synthetic model shows that the dispersion seen in the P-wave arrivals from these events is explained well by the best fitting model described above. The model captures the variation in the spectrogram seen for the events of different depths well. The broad features of the velocity spectra are also reproduced well. The quality of the fit for these shallower events suggests that there is no detectable variation in the bulk properties of the low velocity structure of the slab with depth.

## 5. Discussion

The results presented here offer a new constraint on the fine scale velocity structure of the subducting Nazca plate beneath Northern Chile, and suggest that the low velocity structures related to both metastable oceanic crust, and hydrated lithospheric mantle persists to depths of at least 220 km. Previous guided wave studies in this region have suggested that a single 2–4 km thick LVL of un-metamorphosed oceanic crust may persist to depths of at least 160 km (Martin et al., 2003; Martin and Rietbrock, 2006). In this study we confirm the persistence of a thin LVL of approximately 1 km thickness, and suggest that this LVL may persist to at least 220 km depth.

Additionally we show that in order for the clear P-wave dispersion to be observed, the LVL must be accompanied by low velocity fault zone structure within the lithospheric mantle of the subducting plate. Although we cannot completely rule out alternative scattering models, we propose that the most likely explanation

for this scattering structure is serpentinisation of the lithospheric mantle due to normal faulting at the outer rise. This interpretation is supported by a wide range of geophysical observations suggesting normal faulting is pervasive at the outer rise in Northern Chile (Ranero and Sallares, 2004; Ranero et al., 2005), and other similar subduction zones e.g. Ranero et al. (2003), Grevenmeyer et al. (2005), Naif et al. (2015).

### 5.1. Low velocity fault zone structure in the subducting slab

It has been shown that the introduction of low velocity dipping normal faults significantly improves the match between the synthetic and observed waveforms (e.g. Fig. 2). Similar scattering structures have been inferred in subducted oceanic lithosphere beneath Northern Japan, and two main hypotheses have been suggested to explain the strong P-wave coda seen here. The first attributes the low velocity scattering structures produced during the formation of the oceanic plate (e.g. Furumura and Kennett, 2005). The second attributes the scattering structure to low velocity structure introduced at the outer rise due to normal faults hydrating the oceanic lithosphere as the plate bends (Garth and Rietbrock, 2014b). Previous studies have shown that the P-wave coda is relatively insensitive to the orientation of the scattering material (Garth and Rietbrock, 2014b), therefore we cannot rule out either model from the observations presented. In Northern Chile however normal faults are clearly observed at the outer rise (Ranero et al., 2005), and there is evidence these structures are reactivated at depth (Ranero et al., 2005; Fuenzalida et al., 2013). There is also strong evidence that hydration due to outer rise faulting causes a significant drop in P-wave velocity as the plate bends into the subduction zone

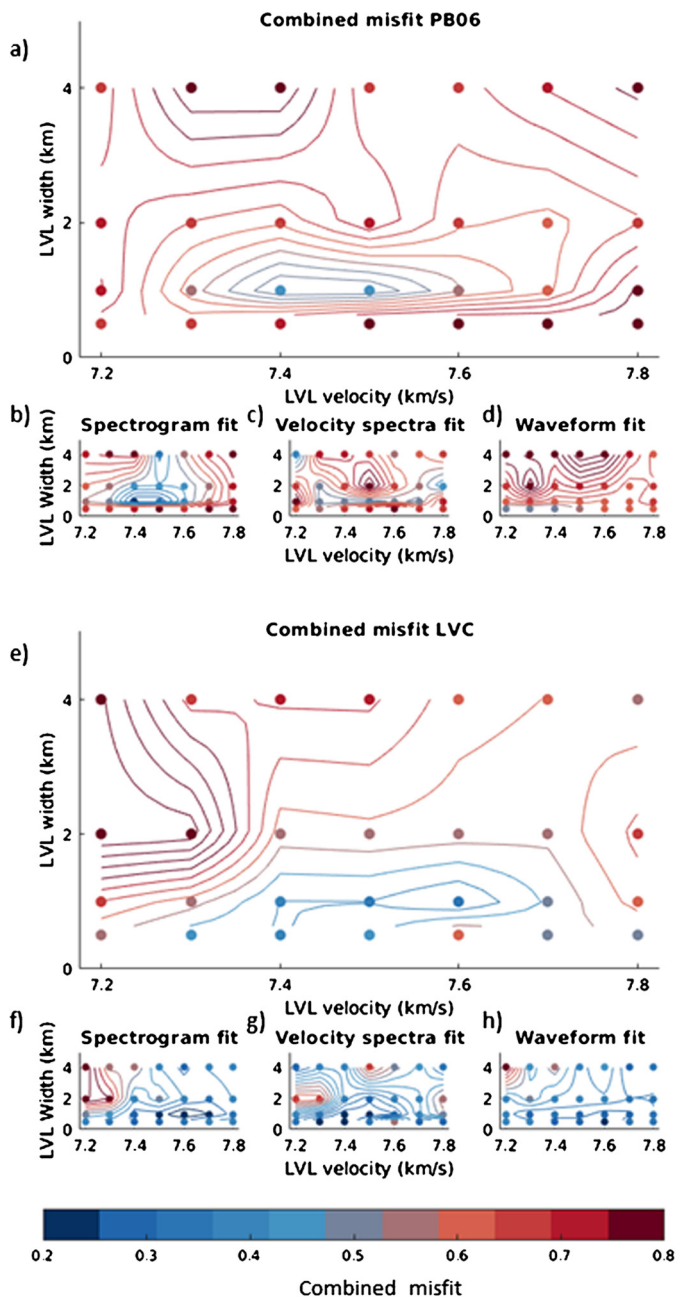


**Fig. 7.** Grid search to constrain the velocity and width of the LVL. **a)** Shows the combined misfit at station PB06. The percentage misfit in the spectrogram **(b)**, velocity spectra **(c)** and low pass filtered waveform **(d)** are shown for the event recorded at station PB06. The combined misfit, spectrogram velocity spectra and waveform misfit are shown in panels **e)–h)** for the station LVC.

(Ranero and Sallares, 2004). We therefore propose that the dominant cause of the low velocity scattering structure inferred within the subducting Nazca plate can be attributed to this outer rise hydration.

This study shows that the serpentinised normal faults that cause the reduced velocities at the outer rise and act as fluid pathways as the plate subducts, may persist as distinct low velocity structures within the slab to depths of at least 220 km. The observation that both a layer of low velocity material at the top of the subducted slab and dipping low velocity normal faults within the subducted slab mantle, suggests that the pervasive WBZ earthquakes at depths of up to ~250 km occur in close proximity to low velocity and potentially hydrous mineral assemblages.

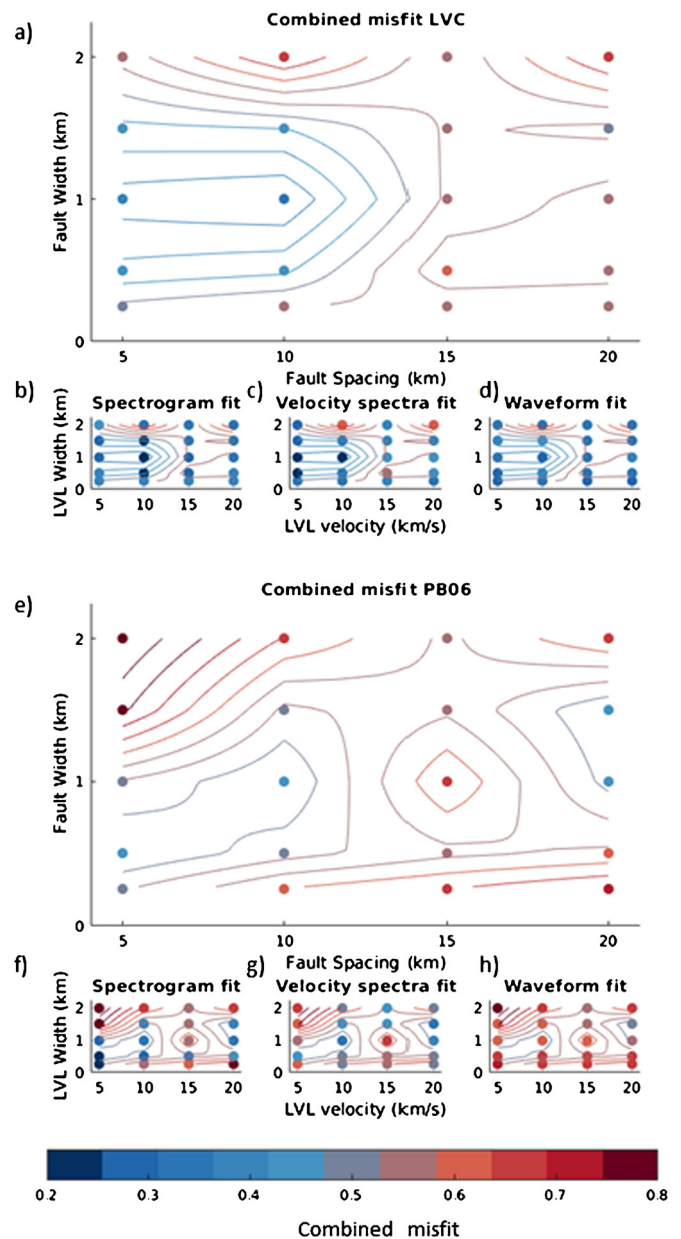


**Fig. 8.** Grid search to constrain characteristics of low velocity fault zones in the lithospheric mantle of the subducting Nazca plate. **a)** Shows the combined misfit at station PB06. The percentage misfit in the spectrogram **(b)**, velocity spectra **(c)** and low pass filtered waveform **(d)** are shown for the event recorded at station PB06. The combined misfit, spectrogram velocity spectra and waveform misfit are shown in panels **e)–h)** for the station LVC.

## 5.2. Comparison with predicted mineral velocities

To interpret the inferred velocity structure, we calculate theoretical P-wave velocities for possible mineral assemblages expected to be present within the oceanic crust and hydrated upper lithospheric mantle (e.g. Hacker et al., 2003a, 2003b). P-wave velocities are calculated at up to 250 km depth for MORB mineral assemblages predicted to be stable at different pressure–temperature (P–T) conditions within the subducting slab and are shown in Fig. 9. The velocities of serpentinised and un-hydrated mantle material are also calculated for the relevant depths. The velocities and water contents of the relevant phases are calculated using the Excel macro of Hacker and Abers (2004) together with the predicted P–T path for subducting Nazca plate beneath Northern Chile of Syracuse et al. (2010). The resulting velocities are compared with



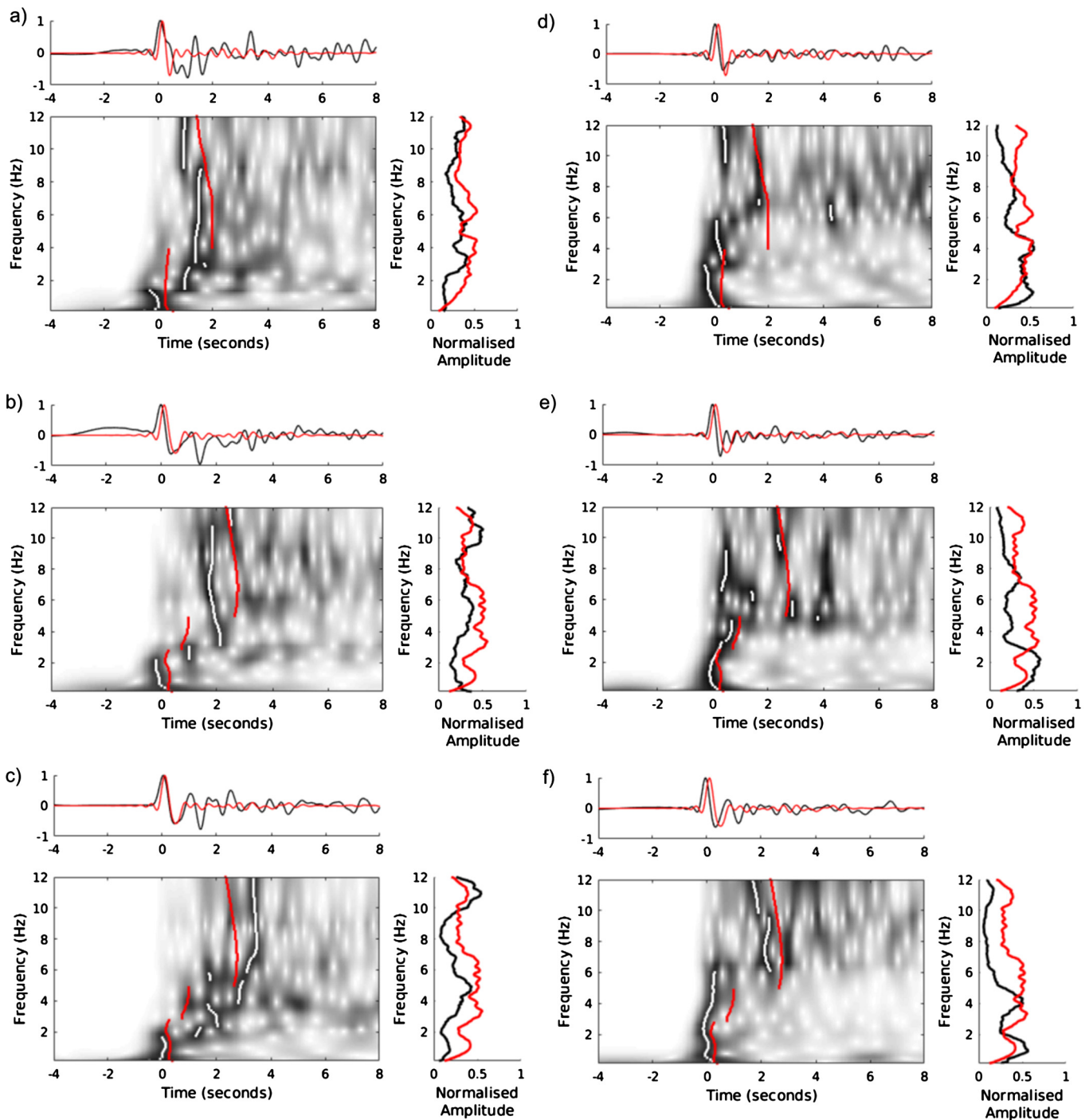


**Fig. 9.** Observed and modelled dispersive waveforms for events at **a)** 140, **b)** 210, and **c)** 220 km depth observed at station PB06. The corresponding arrivals observed at LVC are shown for events at **d)** 140, **e)** 210 and **f)** 220 km depth. The panels of the plot are described in Fig. 3.

the best fitting velocities inferred for the thin LVL as shown in Fig. 10.

The velocities seen are significantly lower than the eclogite phases that are predicted to be stable at these P–T conditions, and are comparable with hydrated lawsonite bearing MORB mineral assemblages such as a jadeite lawsonite blueschist. Guided wave observations from several events at different depths give constraints on different parts the velocity structure at 140–220 km depth, and can be modelled by a constant LVL velocity of 7.5 km/s. Our observations therefore do not detect any significant velocity changes in this depth range. It is noted that the same width of LVL accounts for the dispersion observed from events of different depths, sug-

gesting that the width of the low velocity waveguide also does not change significantly within this depth range.

These new observations imply that a seismically distinct part of the oceanic crust remains unreacted to depths of at least 220 km, well beyond the P–T conditions where eclogite facies are thought to be stable. The velocities inferred suggest that the LVL may consist of metastable lawsonite bearing MORB phases. Previous guided wave studies in Northern Chile have suggested that the thin LVL may be explained by anhydrous gabbros, that remain unreacted due to a lack of water to catalyse the reaction (Martin et al., 2003; Martin and Rietbrock, 2006). Given the large amount of water suggested to be present in the serpentinised lithospheric mantle this

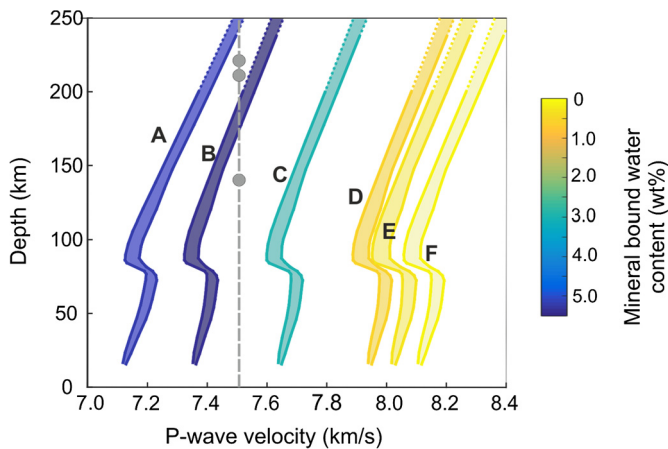


**Fig. 10.** Comparison of mineral velocities with LVL velocities calculated for the top of the Nazca plate (Hacker et al., 2003a). The colours represent the hydration of the given MORB mineral assemblages, and are labelled as follows. (A) lawsonite blueschist, (B) jadeite lawsonite blueschist, (C) lawsonite Amphibole eclogite, (D) Amphibole eclogite, (E) Zoesite eclogite and (F) Eclogite. The grey circles show the velocity of the LVL inferred for individual events. (For interpretation of the colours in this figure, the reader is referred to the web version of this article.)

model seems less favourable. It also seems unlikely that the upper LVL itself can be explained by a serpentinite layer, as the reduced S-wave velocities associated with this are not seen in high resolution receiver function studies of the area (Yuan et al., 2000).

We therefore propose the alternative explanation that the deep LVL can be explained by metastable lawsonite that persists into the stability field of eclogite phases due to a lack of activation energy to trigger the metamorphic reaction. In the subducted Nazca plate the lower part of the oceanic crust may remain unreacted even when the upper crust has been eclogitised as the activation energy required will be higher for the coarser grained gabbros of the lower crust. A similar deep LVL, proposed to consist of unreacted hydrated MORB is inferred from guided wave observations in Northern Japan (Garth and Rietbrock, 2014a). In Japan however the unreacted layer is inferred to be ~8 km thick, suggesting that the eclogite transformation is delayed for the whole of the oceanic crust. This is likely to be due to the much warmer P–T path that the subducting Nazca plate is exposed to, allowing the eclogite reactions to occur faster. Global studies of guided wave dispersion suggest that LVL of 2–8 km thickness may persist to depths >150 km, at several subduction zones in the Pacific (Abers, 2000, 2005). This would imply that the delay in onset of the eclogite transformation may be a common feature in a broad range of subduction zone environments.

### 5.3. Constraining the hydration of the lithospheric mantle

Many studies have suggested that the lithospheric mantle is highly hydrated at the outer rise as the plate bends into the subduction zone. In Northern Chile this is evident from the reduction in P-wave velocity observed from active source seismic experiments at the outer rise (Ranero and Sallares, 2004). Within this region it is also proposed that outer rise faults are reactivated in intermediate depth earthquakes, suggesting that these structures persist to these depths (Ranero et al., 2005).

The results presented here provide the first direct evidence that normal fault structures may be present as distinct low velocity structures at intermediate depth within the subducted slab beneath Northern Chile. The low velocity fault structures are assumed to consist of serpentinitised mantle material, surrounded by un-hydrated mantle. The seismic velocity of the serpentinitised and un-serpentinitised mantle is calculated for P–T conditions of the subducting Nazca plate in Northern Chile, as described above.

These velocities are then used to calculate the bulk serpentinitisation, and therefore hydration of the subducted lithospheric mantle based on the average velocity of the faulted lithospheric mantle in the best fitting models. The observations suggest that the lithospheric mantle is highly hydrated by low velocity normal fault structures, and that the lithospheric mantle is on average 4.7–15.4% serpentinitised. This compares to an estimated serpentinitisation at the outer rise of 17.0% (Ranero and Sallares, 2004).

Using the serpentinitisation constrained in this study, and assuming that the water content of serpentinite is 12.3 wt% (Hacker and Abers, 2004), and the thickness of the WBZ is 11 km, we calculate that the amount of water carried in the hydrated slab mantle is 13–42 Tg/Myr per metre of arc. These results therefore provide a unique in situ constraint on the hydration of the lithospheric mantle at these depths in the 44 Ma old subducting Nazca plate.

### 5.4. Water delivered beyond the main volcanic arc

As these features are constrained at 140–220 km depth, it is likely that much of the water carried in the serpentinitised lithospheric mantle is transported beyond the volcanic arc, to the deeper mantle. The persistence of unreacted oceanic crust, forming the inferred LVL, suggests that mineral bound water in unreacted oceanic crust may also transport some water to the deeper mantle. The presence of mineral bound water beyond the main volcanic arc may account for deeper WBZ seismicity that is seen in this part of the oceanic crust. Water released from the eclogitisation of metastable oceanic crust at these depths may also account for the persistence of the high attenuation mantle wedge and associated volcanic activity seen anomalously far from the trench in this area (Schurr et al., 2003).

Much of the water carried by the subducting Nazca plate is however carried by the serpentinitised lithospheric mantle, and the cooler conditions in the centre of the slab may mean that much of this water is delivered to even greater depth within the mantle. The processes by which the water within the slab is retained or released beyond the stability field of serpentinite are not well understood. Potentially fluids released by the dehydration of serpentinite may be channelled up the subducted oceanic crust, and released to the mantle wedge (e.g. Hacker et al., 2003b; Faccenda et al., 2012), though some fluids retained within the centre of the slab may be carried to the deeper mantle (Faccenda et al., 2012). Alternatively high pressure hydro-silicates may provide a mechanism to transport some of the water as deep as the mantle transition zone (Rüpke et al., 2004).

The observations presented here suggest that subducting oceanic plates of intermediate age, such as the Nazca plate are able to transport significant amounts of water beyond the volcanic arc, and potentially to the deeper mantle. However the results suggest that the lithospheric mantle of the 44 Ma Nazca plate is less hydrated than the 120 Ma subducting lithosphere studied in Northern Japan (Garth and Rietbrock, 2014b). This is consistent with observations of hydration at the outer rise, where a lesser degree of serpentinitisation is seen at young subduction zones such as the ~14 Ma Central Chile (9% serpentinitisation, Contreras-Reyes et al., 2007), and 24 Ma Nicaraguan (12–17% serpentinitisation, Contreras-Reyes et al., 2007; Ivandic et al., 2008) than at older subduction zones such as 90 Ma Tonga (25% serpentinitisation, Contreras-Reyes et al., 2011). Subducting plates with intermediate ages, such as the Nazca plate subducting beneath Northern Chile and the 50 Ma Pacific plate subducting beneath Alaska show similar serpentinitisations of 16–17% (Ranero and Sallares, 2004; Shillington et al., 2015).

These values are consistent with the upper end of estimated hydration produced here for the slab at intermediate depths, while the lower end of the estimates suggests that the slab is less hy-

drated at these intermediate depths, than at the outer rise. The method used here is however primarily sensitive to the large scale structures, and potential smaller water bearing structures are not accounted for.

## 6. Conclusions

Guided wave observations suggest that low velocity structures related to hydration at the outer rise may be present in the lithospheric mantle at intermediate depths, in addition to a thin LVL previously inferred. Dispersed P-wave arrivals from earthquakes at a range of depths suggest that the low velocity structures are on average approximately 8.5% slower than the surrounding mantle material. The velocity of the thin LVL compares to velocities expected for lawsonite bearing MORB mineral assemblages at these depths. This suggests that a part of the oceanic crust may remain un-eclogitized to depths of at least 220 km. Our observations therefore suggest that most if not all intermediate depth WBZ earthquakes in the subducted Nazca plate may occur within close proximity to low velocity structures within the subducted slab.

The observation that hydration due to outer rise faulting persists to at least 220 km, combined with the observation that part of the hydrated oceanic crust remains unreacted to these depths suggest that significant amounts of water may be transported beyond the volcanic arc by relatively young plates such as the Nazca plate. The thinner WBZ, and lower serpentinisation inferred in the subducted Nazca suggest that younger plates transport less water to the mantle than older plates such as those seen in Northern Japan (Garth and Rietbrock, 2014b), however plates of this age are still able to transport significant amounts of water to the deeper mantle. Given that nearly a third (32.5%) of oceanic lithosphere being subducted around the globe today is 40–60 Ma, hydrated oceanic plates, of this age can potentially account for a significant amount of the water that is delivered to the deep mantle.

## Acknowledgements

This work was supported by NERC (grant number 189 NE/H524722/1) and the EU funded VERCE project (project number 283543). Waveform simulations were run on the UK national supercomputer ARCHER. Seismic data was used from Global Seismic Network stations, distributed by IRIS (Incorporated Research Institutions for Seismology). Bathymetric data shown is taken from the GEMCO Digital Atlas published by the British Oceanographic Data Centre.

## References

- Abers, G.A., 2000. Hydrated subducted crust at 100–250 km depth. *Earth Planet. Sci. Lett.* 176 (3), 323–330.
- Abers, G.A., 2005. Seismic low-velocity layer at the top of subducting slabs: observations, predictions, and systematics. *Phys. Earth Planet. Inter.* 149 (1), 7–29.
- Bohlen, T., 2002. Parallel 3-D viscoelastic finite difference seismic modelling. *Comput. Geosci.* 28 (8), 887–899.
- Contreras-Reyes, E., et al., 2007. Alteration of the subducting oceanic lithosphere at the southern central Chile trench-outer rise. *Geochem. Geophys. Geosyst.* 8 (7).
- Contreras-Reyes, E., et al., 2011. Deep seismic structure of the Tonga subduction zone: implications for mantle hydration, tectonic erosion, and arc magmatism. *J. Geophys. Res., Solid Earth* 116 (B10).
- Faccenda, M., Gerya, T.V., Burlini, L., 2009. Deep slab hydration induced by bending-related variations in tectonic pressure. *Nat. Geosci.* 2 (11), 790–793.
- Faccenda, M., et al., 2012. Fluid flow during slab unbending and dehydration: implications for intermediate-depth seismicity, slab weakening and deep water recycling. *Geochem. Geophys. Geosyst.* 13 (1).
- Fuenzalida, A., et al., 2013. High-resolution relocation and mechanism of aftershocks of the 2007 Tocopilla (Chile) earthquake. *Geophys. J. Int.* 194 (2), 1216–1228.
- Furumura, T., Kennett, B., 2005. Subduction zone guided waves and the heterogeneity structure of the subducted plate: intensity anomalies in northern Japan. *J. Geophys. Res., Solid Earth* 110 (B10).
- Garth, T., Rietbrock, A., 2014a. Downdip velocity changes in subducted oceanic crust beneath Northern Japan—insights from guided waves. *Geophys. J. Int.* 198 (3), 1342–1358.
- Garth, T., Rietbrock, A., 2014b. Order of magnitude increase in subducted H<sub>2</sub>O due to hydrated normal faults within the Wadati-Benioff zone. *Geology* 42 (3), 207–210.
- GFZ German Research Centre for Geosciences, Institut des Sciences de l'Univers-Centre National de la Recherche CNRS-INSU, 2006. IPOC Seismic Network. Integrated Plate boundary Observatory Chile – IPOC. Other/Seismic Network. <http://dx.doi.org/10.14470/PK615318>.
- Graeber, F.M., Asch, G., 1999. Three-dimensional models of P wave velocity and P-to-S velocity ratio in the southern central Andes by simultaneous inversion of local earthquake data. *J. Geophys. Res., Solid Earth* 104 (B9), 20237–20256.
- Grevemeyer, I., et al., 2005. Heat flow and bending-related faulting at subduction trenches: case studies offshore of Nicaragua and Central Chile. *Earth Planet. Sci. Lett.* 236 (1), 238–248.
- Hacker, B.R., Abers, G.A., 2004. Subduction Factory 3: An Excel worksheet and macro for calculating the densities, seismic wave speeds, and H<sub>2</sub>O contents of minerals and rocks at pressure and temperature. *Geochem. Geophys. Geosyst.* 5 (1).
- Hacker, B.R., Abers, G.A., Peacock, S.M., 2003a. Subduction factory 1. Theoretical mineralogy, densities, seismic wave speeds, and H<sub>2</sub>O contents. *J. Geophys. Res., Solid Earth* 108 (B1).
- Hacker, B.R., et al., 2003b. Subduction factory 2. Are intermediate-depth earthquakes in subducting slabs linked to metamorphic dehydration reactions? *J. Geophys. Res., Solid Earth* 108 (B1).
- Hayes, G.P., Wald, D.J., Johnson, R.L., 2012. Slab1.0: a three-dimensional model of global subduction zone geometries. *J. Geophys. Res., Solid Earth* 117 (B1).
- International Seismological Centre, 2014. On-line bulletin. *Internatl. Seismol. Cent., Thatcham, United Kingdom*. <http://www.isc.ac.uk>.
- Ivandić, M., et al., 2008. Impact of bending related faulting on the seismic properties of the incoming oceanic plate offshore of Nicaragua. *J. Geophys. Res., Solid Earth* 113 (B5).
- Martin, S., Haberland, C., Rietbrock, A., 2005. Forearc decoupling of guided waves in the Chile–Peru subduction zone. *Geophys. Res. Lett.* 32 (23).
- Martin, S., Rietbrock, A., 2006. Guided waves at subduction zones: dependencies on slab geometry, receiver locations and earthquake sources. *Geophys. J. Int.* 167 (2), 693–704.
- Martin, S., et al., 2003. Guided waves propagating in subducted oceanic crust. *J. Geophys. Res., Solid Earth* 108 (B11).
- Naif, S., et al., 2015. Water-rich bending faults at the Middle America Trench. *Geochem. Geophys. Geosyst.* 16 (8), 2582–2597.
- Peacock, S.M., 2001. Are the lower planes of double seismic zones caused by serpentine dehydration in subducting oceanic mantle? *Geology* 29 (4), 299–302.
- Ranero, C., Sallares, V., 2004. Geophysical evidence for hydration of the crust and mantle of the Nazca plate during bending at the north Chile trench. *Geology* 32 (7), 549–552.
- Ranero, C.R., et al., 2003. Bending-related faulting and mantle serpentinization at the Middle America trench. *Nature* 425 (6956), 367–373.
- Ranero, C.R., et al., 2005. Relationship between bend-faulting at trenches and intermediate-depth seismicity. *Geochem. Geophys. Geosyst.* 6 (12).
- Rietbrock, A., Waldhauser, F., 2004. A narrowly spaced double-seismic zone in the subducting Nazca Plate. *Geophys. Res. Lett.* 31 (10).
- Rüpke, L.H., et al., 2004. Serpentine and the subduction zone water cycle. *Earth Planet. Sci. Lett.* 223 (1), 17–34.
- Schurr, B., et al., 2003. Complex patterns of fluid and melt transport in the central Andean subduction zone revealed by attenuation tomography. *Earth Planet. Sci. Lett.* 215 (1), 105–119.
- Shillington, D.J., et al., 2015. Link between plate fabric, hydration and subduction zone seismicity in Alaska. *Nat. Geosci.* 8 (12), 961–964.
- Syracuse, E.M., Abers, G.A., 2006. Global compilation of variations in slab depth beneath arc volcanoes and implications. *Geochem. Geophys. Geosyst.* 7 (5).
- Syracuse, E.M., van Keken, P.E., Abers, G.A., 2010. The global range of subduction zone thermal models. *Phys. Earth Planet. Inter.* 183 (1), 73–90.
- van Keken, P.E., et al., 2011. Subduction factory: 4. Depth-dependent flux of H<sub>2</sub>O from subducting slabs worldwide. *J. Geophys. Res., Solid Earth* 116 (B1).
- West, M., Christensen, D., 2010. Investigating the Relationship Between Pluton Growth and Volcanism at Two Active Intrusions in the Central Andes. *International Federation of Digital Seismograph Networks*.
- Yuan, X., et al., 2000. Subduction and collision processes in the Central Andes constrained by converted seismic phases. *Nature* 408 (6815), 958–961.